3D printing in situ gelification of κ-carrageenan solutions: effect of printing variables on the rheological response

I. Diañez[a], C. Gallegos[b], E. Brito-de la Fuente[b], I. Martínez[a,c], C. Valencia[a,c], M.C. Sánchez[a,c], M.J. Diaz[a,c], J.M. Franco[a,c,✉]

[a] Dept. Ingeniería Química, Universidad de Huelva, Campus de El Carmen, 21071 Huelva, Spain

[b] Product & Process Engineering Centre, Fresenius Kabi Deutschland GmbH, 61352 Bad Homburg, Germany

[c] Chemical Process and Product Technology Research Centre (Pro2TecS), 21071 Huelva, Spain

✉ Corresponding author:
Prof. J.M. Franco. E-mail: franco@uhu.es

ABSTRACT

This work reports a successful 3D printing-based in situ temperature-induced gelification procedure of κ-carrageenan aqueous dispersions. 3D printer was modified to handle low viscosity fluid feeding and more efficiently distribute ambient air at room temperature causing forced convection to accelerate the cooling of the printed layer. Thus, obtained gel samples, containing 30 mg/g κ-carrageenan in water, showed self-sustaining capability and a rheological response comparable with a reference conventionally prepared gel. Moreover, the effect of main printing variables, such as temperature of the hotend, printing speed and layer height, on the linear viscoelastic response of the gels was analysed by application of the response surface methodology (RSM). In general, gel strength linearly increases by decreasing printing speed and layer height whereas not noticeable improvement in gel strength was achieved by applying hotend temperatures above 80-85 °C. Based on the results obtained from this analysis, an optimisation method is proposed to minimise the temperature and time needed to 3D print a gel with pre-set rheological properties. Overall, this study demonstrates that it is possible to generate in situ 3D printed gel materials with potential uses in food and pharmaco-nutrition, without the aid of reactive additives or initiators, and using a facile protocol.

Keywords:

3D printing, additive manufacturing, κ-carrageenan, food design, gel, Rheology

1. Introduction

3D printing is becoming a more important part of our lives every day, apart from already being used industrially, due to the wide variety of possibilities that it can deliver, especially in the development of customised and innovative products. There are several technologies that can be included in the category of 3D printing or additive manufacturing. However, those based on fused filament fabrication are probably the most extended, being suitable for a huge range of applications and materials (Jose, Rodriguez, Dixon, Omenetto, & Kaplan, 2016; Ren, Shao, Lin, & Zheng, 2016; Wegrzyn, Golding, & Archer, 2012). Additive manufacturing refers to the process of building a 3D object by adding layer-upon-layer materials, such as plastic, metal, concrete…, or any material capable of forming stable self-supporting structures. The simplicity of this process is what makes it so versatile, since it does not need the use of materials with special reactive properties and/or initiators. In this context, many industries are focusing their interest on adapting 3D printing technology to the specific needs of each sector. Among many other fields, food processing, gastronomy and cooking are showing growing interest in 3D printing technologies (Lipton, Cutler, Nigl, Cohen, & Lipson, 2015; Pallottino et al., 2016; Sun et al., 2015; Sun, Zhou, Huang, Fuh, & Hong, 2015; Sun, Zhou, Yan, Huang, & Lin, 2018). In one hand, it can be used in food industry for the development of new products (Godoi, Prakash, & Bhandari, 2016; Lipton et al., 2015). Moreover, it could also be the next cooking utensil present in our kitchens, as blenders or toasters are nowadays (Izdebska & Zołek-Tryznowska, 2016). Beyond this, 3D printing can become an useful tool for pharmaceutical and clinical nutrition industries, since it could be a way to process fully customisable products, according to the needs of each specific patient (Severini & Derossi, 2016; Sun et al., 2018), e.g. in the design of personalised foods for dysphagia management. In addition, the in situ product manufacture, just before administration or use, may solve some problems related to storage of unstable or incompatible components.

In all these fields, materials with specific gel characteristics are of great importance. Particularly interesting to form hydrogels is κ-carrageenan, which is considered a representative gel forming polysaccharide, with thermoreversible gelling capacity and widely extended use in many applications, especially in the food, pharmaceutical and cosmetic industries (Ikeda & Nishinari, 2001; Liu, Huang, & Li, 2016). As well-known, κ-carrageenan is a sulphated polysaccharide extracted from different species of red seaweed (Yang, Yang, & Yang, 2017), which needs to be heated and then cooled to gelify, what is known as “cold-setting” (Piculell, 2006). It is well accepted the two-step gelation mechanism involving the formation of helical dimers first, as proposed by Rochas and Rinaudo (Rochas & Rinaudo, 1982), followed by the aggregation of double helices (Iijima, Takahashi, Hatakeyama, & Hatakeyama, 2013; Mangione, Giacomazza, Bulone, Martorana, & San Biagio, 2003).

In this aggregation process, the molecular chains extend and associate to other molecules favouring the formation of a three-dimensional network composed of double-helical aggregates as the junctions and flexible chains connecting the junctions (Iijima et al., 2013; Liu, Chan, & Li, 2015). To induce the gelation of κ-carrageenan in water, the temperature must be increased, yielding the hydration and swelling of particles in a range of between 40 and 60 °C, which causes an increase in its viscosity. Afterwards, between 70 and 80 °C, a further drop in viscosity occurs, due to the carrageenan molecules being organised in randomly arranged coils (Imeson, 2009). Typical procedures to prepare κ-carrageenan gels deal with heating at 70-90 °C under stirring for 30 min to 2h (Ikeda & Nishinari, 2001; Liu et al., 2015; Yang et al., 2017). When the solution is cooled down, these coils are structured giving rise to the formation of the gel network (Ikeda & Nishinari, 2001; Imeson, 2009). Then, a thermal hysteresis is apparent in subsequent heating and cooling cycles above a critical concentration (Yang et al., 2017), being the melting temperature higher than the gelling temperature. However, as well known, the κ-carragenan gelification process is highly dependent on salt concentration and nature of the cations (Funami et al., 2007; Hermansson, Eriksson, & Jordansson, 1991; Thrimawithana, Young, Dunstan, & Alany, 2010). The need for all these thermal steps to take place in order to produce gelification complicates the use of continuous processes, as is the case of 3D printing. In addition, the specific conditions under which gelling takes place can lead to structures with different properties (Cavallieri, Fialho, & Cunha, 2011; Cooke et al., 2018). In this sense, rheology is presented as a powerful tool to assess the gel characteristics and final performance as a gel matrix in more complex formulations (Liu et al., 2015). The possibility of preparing gel matrices with tailored rheological properties using efficient, quick and facile protocols is a big challenge that can be achieved by properly adapting the 3D printing technology. For instance, in the case of κ-carrageenan gels, it is worth mentioning that the transition from random coil to double helices is extremely fast (Norton, Goodall, Morris, & Rees, 1983). However, subsequent aggregation of double helices to complete the formation of a gel three dimensional network may take up to 15 h (Tecante & Doublier, 1999).

Up to now, the application of 3D printing in gel food processing has been mainly limited to extrude with sophisticated shapes previously gellified systems (Chinga-Carrasco et al., 2018; Holland, Tuck, & Foster, 2018; Wang, Zhang, Bhandari, & Yang, 2018) or, in the best cases, a viscoelastic dispersion or solution (Vancauwenberghe et al., 2017). Only a few works on 3D printing-induced gelation, i.e. the so-called 3D gel printing, have been reported for non-food systems (Moxon et al., 2017; Zhu et al., 2016) and most of them required a catalyst or initiator (Ren et al., 2016). It is apparent that 3D printing-induced gelation could also have a relevant application for designing alternative, alpha-

amylase-resistant, customised "fresh" pudding-like products for nutritional support of dysphagia patients (Gallegos, Brito-de la Fuente, Clavé, Costa, & Assegehegn, 2017; Turcanu et al., 2018).

Taking into account these considerations, the aim of this study was to take advantage of the potential and versatility of the 3D printing technology to induce the in situ gelification of κ-carrageenan aqueous solutions, subsequently studying, by means of a RSM experimental design, the influence of the main 3D printing variables on the rheological properties of the gel matrices obtained.

2. Experimental

2.1. Materials

κ-carrageenan (M_W 193 - 324 kDa, K ≤ 110 mg/g, Ca ≤ 35 mg/g, Na ≤ 20 mg/g, moisture ≤ 120 mg/g) was used as received from Sigma-Aldrich (Germany). Water was directly taken from the Huelva water supply network, with an average content of cations of Ca 15.7±2 mg/L, Mg 10.5±1.4 mg/L, Na 29.9±3.6 mg/L, K < 2 mg/L (Ayuntamiento de Huelva, 2015; ENAC, 2017). The content and proportions of cations have not been modified during the study to avoid interferences with the effects caused by the variation of the printing parameters.

2.2. Preparation of κ-carrageenan hydrogels

κ-carrageenan hydrogels studied were prepared by 3D printing. A BQ Hephestos 3D printer DIY kit, with Marlin-derived firmware designed by BQ (Spain), was used for this study once previously adapted and submitted to modifications to print liquid feeds, as described in section 3. All the additional components needed for its adaptation were supplied by 3DEspaña (Spain). 3D printer feeding premix was directly prepared by dispersing 30 mg/g κ-carrageenan in water at room temperature under vigorous mixing (1500 rpm), for 30 min, with a magnetic stirrer, without any other supplement of cations, aiming to reproduce ordinary homemade preparations. These dispersions were fed on demand to the printer through a syringe pump system and gellified in situ during the 3D printing process. Main printing variables (printing speed, hotend temperature and layer height) were modified according to the experimental design described below. Carrageenan gel discs of 50 mm diameter and 1 mm height were printed for rheological characterization. The different shapes and models printed during this study, as well as all accessories required to modify the printer, were designed using AutoCAD 2018 software and Tinkercad online app. The slicing of the 3D models, necessary to obtain the .gcode extension files with all the information the printer needs to run, was carried out with Ultimaker Cura software and control of the 3D printer during operation was made possible by Repetier Host software.

In addition, a reference hydrogel sample was prepared from the same 30 mg/g carrageenan dispersion employed to feed the printer, using a conventional protocol (Liu et al., 2015, 2016). The carrageenan dispersion was heated by means of a heating plate at 80 °C for 2 h in a closed vessel, under vigorous stirring (1500 rpm) and then cooled down to room temperature by natural convection.

2.3. Rheological characterization

Rheological characterisation of gel samples was carried out with a controlled stress rheometer (Physica MCR-301, Anton Paar, Austria). Small-amplitude oscillatory shear (SAOS) tests were performed inside the linear viscoelastic region, using a plate-plate geometry (25 mm diameter, 1 mm gap) in a frequency range of 0.03-100 rad/s, at 25 °C. The 50 mm diameter gel discs directly obtained by 3D printing were placed on the rheometer geometry and the excess sample was carefully removed to suit the 25 mm plate diameter.

2.4. Experimental design and statistical analysis

The main printing parameters that have been considered throughout this study are the hotend temperature (T), printing speed (S) and layer height (H). The temperature of the hotend is the temperature of the heating block, which can be set to the desired value and measured continuously; the printing speed is the speed corresponding to the displacement movement of the hotend during the deposition of the material; and the layer height is the thickness of each of these deposited layers. In order to determine the effect of these printing parameters and the interactions between them on the rheological response of the carrageenan gels, with the minimum possible number of experiments, a response surface methodology (RSM) experimental design was applied. In particular, a Box-Wilson three factors circumscribed central composite design (CCC) at 5 levels of each factor, with an α-value of ±1.682. Several replicates of the central point of the cube were carried out, with additional experiments lying at the cube vertices and side centres, originating 20 different case studies, which were rheologically characterized.

This experimental design enables the construction of second-order polynomials in the independent variables, as shown below:

$$Y = a + a_1x_1 + a_2x_2 + a_3x_3 + a_{12}x_1x_2 + a_{13}x_1x_3 + a_{23}x_2x_3 + a_{11}{x_1}^2 + a_{22}{x_2}^2 + a_{33}{x_3}^2 \quad (1)$$

Being Y the dependent variable, x_i the normalised values of the independent variables and a_{ij} the constants obtained from regression analysis.

In this way, a regression analysis was carried out on selected rheological parameters (see eq. 4 parameters defined below) as dependent variables and the printing parameters (printing speed, hotend temperature and layer height) as independent variables. Those variables whose significance level exceeds 0.05 in Student's *t* test were excluded from the analysis and the resulting polynomials.

The normalisation of the values of each variable, necessary to be able to compare its influence, was carried out by means of the following equation:

$$X_N = \frac{2\cdot(X - X_{med})}{(X_{max} - X_{min})} \quad (2)$$

Where X_N is the normalised value of the variable, X is its real value, X_{med} is the average value of the variable and X_{max} and X_{min} are the upper and lower limits, respectively, of the range considered for each variable. The range of each variable studied and their normalised values are detailed in Table 1.

3. 3D printer setup

Nowadays, there are many different models of 3D printers available, fully assembled and ready to use, which are marketed by different companies. However, most of them do not allow to either handle fluid feed or to introduce modifications to do it. Moreover, for the moment, their prices can be excessive for private consumers and small businesses or institutions. An alternative that is leading to what may be considered a new industrial revolution is the RepRap 3D printing technology. The RepRap (replicating rapid prototype) project is an initiative dedicated to designing and developing low-cost 3D printers. RepRap 3D printers are based on open-source hardware and software, which are able to print most of their own components, so they can self-replicate and repair themselves, making them freely available for everyone (Wittbrodt et al., 2013). Their design, assembly and operating instructions can be found accessible and fully detailed on the web, as well as their firmware code. Thus, their tuning possibilities are almost unlimited. In fact, RepRap community is now made up of hundreds of collaborators, leading to a continuous open-source research and development activity. Therefore, RepRap appears as a technically and economically viable form of additive layer manufacturing of polymer-based products (Kreiger & Pearce, 2013). Moreover, it has the potential to have a lower environmental impact than conventional manufacturing for a variety of products (Kreiger & Pearce, 2013; Pearce et al., 2010).

The aim of this work was to go a step forward using a RepRap 3D printer instead of fully assembled commercial printers, in order to achieve gel structures through direct sol−gel transition, i.e. the in situ gelification. This requires the addition and/or replacement of some components of the original printer setup. The proposed self-adapted setup consists of a syringe pump that, through a polytetrafluoroethylene (PTFE) tube, feeds a watertight hotend that provokes the gelification of the carrageenan solution by temperature. Since feeding syringe is not attached to the printing head, it is possible to avoid problems associated with excessive inertia during movement, resulting in higher printing accuracy. A picture and a schematic depiction of this setup can be seen in Figure 1. The syringe pump consists of a plastic structure, designed and printed with the printer itself prior to modification, metal rods as guides for its movement and a motor connected directly to the printer

electronics, instead of the motor corresponding to the original extruder. This extruder, prepared to work with plastic filaments, had to be replaced by a Bowden type watertight hotend in order to handle low viscosity fluids. With these modifications, the printer operated as intended and there is no material leakage. Unfortunately, printing definition was very poor and the material flowed when deposited, so that the model was not able to gain height (Figure 2a). After several attempts under different printing conditions, it was concluded that there was not enough time between deposition of the different layers for cooling and structuring of the material, even when the printing speed was greatly reduced. The Bowden-type hotend does not allow to couple a standard layer fan, so there was no cooling system for the printed material apart from exposure to ambient air. Aiming to solve this drawback, a new piece was designed and printed on polylactic acid (PLA). This piece allows the layer fan of the old extruder to be adapted to the new hotend, as well as distributing the air flow evenly thanks to a diffuser ring (see scheme in Figure 2b). This simple cooling system is based on ambient air at room temperature; but the mere fact of causing forced convection is sufficient to accelerate the cooling of the material, allowing the gel to structure in a way that the model can gain height. These modifications resulted in the printing of carrageenan gel models with an acceptable resolution and self-sustaining capability, as shown in Figure 2c (see also movie placed in the Supporting Information). However, the resolution in this case is limited by the nature of the material. When deposited, the material flows until it cools down sufficiently to structure itself. This is the reason why it was not possible to increase the height of the printed gels before the modification of the system with the cooling ring. In the same way, this brief flow of material means that the shapes are not preserved as faithfully as when working with other more conventional solid materials. Dimensions of the star-shaped model printed after optimising the resolution are displayed in Figure 2c.

Due to these changes on the printer setup, the device had to be recalibrated, making some changes to the printer firmware for proper operation. Since the default extruder stepper motor was replaced by the one that drives the syringe pump, it was necessary to modify the value of axis steps per unit so that the feed flow was adequate for the geometry of the new feed system. From the values of printing speed, layer height and nozzle diameter (the same 0.4 mm diameter nozzle has been used for the entire study), the printer automatically adjusts the required material flow. The firmware was configured to give the correct reading of the new hotend thermocouple and the PID control constants for the new heater block were also determined.

4. Results and discussion

4.1. Rheological behaviour

κ-carrageenan gels processed by 3D printing exhibited a qualitatively similar rheological response, characterized by a slight frequency dependence of the storage modulus (G') and a soft minimum in the evolution of the loss modulus (G''), being G' values almost one decade higher than G'' values. Figure 3 shows the evolution of both SAOS functions with frequency for selected 3D printed carrageenan gels. In particular, Figure 3a presents frequency sweeps of several samples, processed at the same speed (35 mm/s) and layer height (0.18 mm) but applying different temperatures at the hotend, compared with a carrageenan gel conventionally prepared at 80 °C. As can be seen, only the sample printed at 50 °C significantly differs from the others. As well known, at such a low temperature, the necessary mobility of the carrageenan coils is not reached in the solution phase and the gel network structure cannot fully develop when it was subsequently cooled. Once the temperature threshold required for the release of the coils has been exceeded, the structures obtained after gelling are quite similar to each other, even if the hotend temperature is significantly increased, i.e. 110 °C. Above this temperature threshold, both 3D printed and conventionally prepared gel samples have a similar rheological response. In fact, the linear viscoelastic functions of the carrageenan prepared in a conventional heating device, for 2 h under mixing, and those corresponding to the sample obtained by 3D printing at 80 °C are practically identical. Figure 3b, on the other hand, illustrates the effect of layer height at the same temperature (80 °C) and printing speed (35 mm/s), while, finally, Figure 3c compares the SAOS functions of printed gels at different speeds, keeping constant both hotend temperature (80 °C) and layer height (0.18 mm). As can be clearly seen, both higher layer height (H) and higher speed (S) lower the viscoelastic moduli over the entire frequency range considered.

The evolution of SAOS functions with frequency obtained in all cases shows a slight decrease in G' when the frequency is reduced, due to the structural rearrangement and relaxation processes undergone by the gel network when it is subjected to a high enough stress. Besides this, moderate differences between G' and G'' values (less than one decade; in most cases, tan δ values higher than 0.1) is typically reported to be characteristic of relatively “weak gels” (Ross-Murphy & Shatwell, 1993). For all the printed gels, the loss tangent exhibited very similar values (tan δ=0.20±0.12) within the whole frequency range studied. For this reason, the complex modulus (G*), defined as:

$$|G^*|^2 = |G'|^2 + |G''|^2 \quad (3)$$

can be selected as an appropriate viscoelastic function to be modelled as a function of the 3D printing variables. G* has been fitted to a power-law model:

$$G^* = A\omega^n \quad (4)$$

where ω is the angular frequency (rad/s) and, according to the basic theory of gels, A represents the gel strength and n is a power-law relaxation exponent (Campo-Deaño & Tovar, 2009; Moresi, Bruno,

& Parente, 2004; Munarin et al., 2014). In physical gelation, it has been widely reported that physical cross-links, i.e. entanglements, may change with time under the application of stress, causing an actual fluctuation in the state of gelation. For these so-called weak gels, Mita and Bholin (Mita & Bohlin, 1983) proposed that the real structure of such materials may be represented as a cooperative arrangement of flow units. In this context, the reciprocal of the above referred power law index, z=1/n, has been defined by different authors as a coordination number (Gabriele, De Cindio, & D'Antona, 2001) that assumes the meaning of the number of rheological units correlated with one other in the three dimensional structure, and applied to different gel systems (Antunes et al., 2008; Basu et al., 2011; Lupi et al., 2015). Therefore, in the present study, the coordination number could be related to the number of interacting rheological units within the 3D gel network, whilst A is a parameter associated to the strength of the interactions between them and therefore may be correlated to the bulk gel strength. An example of fitting of the G* vs. frequency plots to eq. (4) can be seen in Fig. S1, in the "Supporting Information" document.

4.2. Response Surface modelling

Table 2 lists the values of fitting parameters A and z obtained for each case, as well as the normalised values of independent variables. By applying the multivariate regression analysis, parameter A can be described as a function of the independent variables by means of the following equation:

$$A = 11224.0 - 1931.0 \cdot S + 3617.2 \cdot T - 2881.0 \cdot H - 1355.1 \cdot T^2 \quad (5)$$

$$(R^2 = 0.91; F = 37.33; df = 4.15)$$

This means that A linearly decreases with the printing speed (S) and layer height (H), as Fig. 3b and 3c suggest, whereas it depends quadratically on the temperature (T), in the range of printing variables studied. Moreover, good fitting results were obtained without the need to include terms of interaction among variables.

A similar dependence of the printing variables was found on parameter z, which can be modelled as follows:

$$z = 16.48 - 0.84 \cdot S + 1.11 \cdot T - 1.02 \cdot H - 1.82 \cdot T^2 \quad (6)$$

$$(R^2 = 0.93; F = 47.01; df = 4.15)$$

Since independent variables can only be associated with two of the axes of the 3D graphic (the third axis corresponds to the observed dependent variable), the response surfaces are drawn by giving values between -1.682 and +1.682 to two of the independent variables, while the third remains constant (see Figure 4).

4.2.1. Constant layer height (H) plots

As can be deduced from eqs. 5 and 6, A and z are linearly related to H, so that the surfaces corresponding to the different levels of H are parallel and equidistant from each other, as it is shown in Figs. 4a and 4b. As can be seen, parameter A decreases by increasing the layer height. An increase in layer height implies a larger amount of deposited material, so more time is required to cool down a given volume of sample before the next layer is deposited. Therefore, especially at high printing speed, the material does not have enough time to be properly cooled down and the network that is formed exhibits weaker interactions. As a result, the higher the layer height, the lower values of A and z were obtained, which in practice means lower gel strength.

For the same H-value, response surface model predicts a tendency to reach maximum A-values for low speeds and high temperatures, which corresponds to the expected behaviour, since it is the combination under which the material is most exposed to temperature increment, due to the longer residence time and the greater temperature gradient between the fed material and the hotend. As the coil-helix transition temperature is more widely exceeded, the carrageenan chains are more mobile and the creation of the gel structure is favoured upon cooling. However, the values of parameter A are levelled off at around 100 °C, whereas z reaches a maximum at around 80-85 °C. This means that no benefit can be taken by excessively heating the sample; on the contrary, a not so compact gel structure seems to be formed due to a partial non-reversible coil-helix transition and/or not so efficient aggregation of double helices. As Tanaka (Tanaka, 2003) pointed out, different associations of double helices, differing in the number of helices and average helix length, may be achieved at different temperatures. In particular, this theoretical study predicts that the number of helices per chain, which may be related with parameter z in eq. (4), passes through a maximum at a given temperature. In addition, low velocities also allow each layer of deposited material more time to cool down before it is covered by the next layer of hot material. So, the optimum point will be determined by the maximum time (minimum speed) that can be used in printing, ensuring that the limit value that allows the printer to work without clogging problems is reached. In this case, as a water-based material, conditions combining an excessively low flow rate with high temperature (e.g. printing speed below 2 mm/s and temperature above 85 °C) may result in drying of the material and consequent system clogging problems. However, in most applications, the aim is to reduce total printing time and energy consumption, so that operating conditions would be closer to the upper limit: high layer height and printing speed at the lowest possible temperatures.

When hotend temperature is increased enough to allow the dispersion to exceed the hydration and dissolution threshold of carrageenan molecules (above 62-64 °C, see Figure S2 in the Supporting Information), it is not necessary for the material to remain exposed to that temperature for so long, so that printing can be accelerated without major changes in the resulting rheological properties.

337 *4.2.2. Constant printing speed (S) plots*

338 As can be seen in Figs. 4c and 4d, the A and z response surfaces for constant S-values are very similar
339 to those of constant H-values, since the relationship of both independent variables with the
340 dependent variables are linear and comparable (eqs. 5 and 6). Both the layer height and printing
341 speed are related to the material flow, which is being heated inside the hotend, since H determines
342 the amount of material that goes through the 3D printing system and S is related to the hotend
343 residence time. Moreover, once the material has been deposited on printing surface or on the
344 previous layer, there is also an equivalent effect during cooling. The printing speed determines the
345 time the material is cooled and therefore the time during which the material can be properly self-
346 structured, whereas the layer height is related to the amount of material that needs to be self-
347 structured.

348 *4.2.3. Constant temperature (T) plots*

349 Unlike those corresponding to constant H and S values, all graphs constructed for constant T-values
350 are flat surfaces (Figs. 4e and 4f). Moreover, there are no interactions between the variables, so that
351 all surfaces are parallel to each other. As just mentioned, the effects of layer height and print speed
352 are somewhat equivalent. Therefore, the maximum values of A (stronger gel network) and z (higher
353 number on interacting units) are predicted for the lowest values of H and S, while the minimum is
354 exactly at the opposite corner, which tends to zero in the case of A, i.e. extremely low gel
355 consistency. On the other hand, as previously discussed, A values are closer for hotend temperatures
356 around 80-100 °C, and z reaches maximum values at around 80 °C (the higher plane in Fig. 4f).

357 ***4.3. Time as a variable***

358 One of the goals of this study was to elaborate a practical model that allows predicting the
359 rheological response of κ-carrageenan gels as a function of the main 3D printing variables directly
360 involved in its manufacture: layer height, printing speed and temperature of the 3D printer hotend.
361 In a typical product design process, the properties to be achieved would be set and the processing
362 conditions should be established to achieve them at the lowest possible cost. In this context, the
363 temperature would be an easily optimisable variable according to energy consumption: the most
364 appropriate value would be the lowest value able to guarantee the desired final properties. For
365 instance, as previously discussed, not noticeable improvement in gel strength was achieved by
366 applying hotend temperatures above 80-85 °C. However, both layer height and printing speed are
367 more complex to analyse. These variables are necessary to be able to define the conditions of the
368 printing process, but do not have as much effect on the cost of the process as in the case of
369 temperature. Nevertheless, the combination of both of them determines the value of a decisive
370 variable in terms of cost optimization: the printing time.

Both the printer firmware and the software used in this study are the same as when printing with a conventional solid filament. In this way, the system can be treated analogously to a traditional solid filament printing system.

The printing speed, S, is the linear speed of the nozzle when printing. Thus:

$$t = \frac{L}{S} \tag{7}$$

where t is the total printing time and L is the length of the complete path the nozzle has to take to print a certain model. For a constant section 3D printed object, like the discs printed in this work for further rheological assessment of gel models:

$$L = L_c \cdot N_c \tag{8}$$

L_C being the length of the path necessary to print each layer and N_C being the number of layers of the model. By combining both equations (eqs. 7 and 8):

$$t = \frac{L_c \cdot N_c}{S} \tag{9}$$

The number of layers for a certain object would be the total height (h_m) divided by the height of each layer (H). So, the total printing time will be:

$$t = \frac{L_c \cdot h_m}{S \cdot H} \tag{10}$$

In this equation, h_m is a known value (1 mm in the gel discs) and L_C can be calculated from the "filament" length, $L_{filament}$. When the printer is operated conventionally by using a solid plastic filament that melts before being deposited, slicing software provides the length of filament to be used for printing a certain model. This value, included in the .gcode file, is the $L_{filament}$.

This filament is of a known diameter ($d_{filament}$) and, when it melts and passes through the nozzle, its section changes, taking the width of the outlet hole, d_{nozzle}, and the thickness corresponding to the layer height, H. If the volume of the material is considered to be constant before and after the nozzle (regardless of thermal expansion), the length of the filament consumed and the length of the deposited thread will be different. In this case, as it is not a solid filament, the internal diameter of the feed tube (2 mm) is taken as $d_{filament}$.

Thus, known $d_{filament}$ and d_{nozzle}, the $L_{filament}$ value, taken from the .gcode file by analogy with a solid filament, can be used to calculate the length of the deposited thread. Moreover, if the value of $L_{filament}$ is taken as the data corresponding to laminate a single layer of the discs, the value of L_C can be obtained as follows:

$$L_c \cdot d_{nozzle} \cdot H = L_{filament} \cdot \frac{\pi}{4} \cdot \left(d_{filament}\right)^2 \tag{11}$$

$$L_c = \frac{L_{filament} \cdot \frac{\pi}{4} \cdot d_{filament}}{d_{nozzle} \cdot H} = \frac{L_{filament} \cdot \frac{\pi}{4} \cdot (2\ mm)^2}{0.4\ mm \cdot H} = 986.4\ mm \tag{12}$$

When considering discs printed with different H values, $L_{filament}$ also changes (the thicker the deposited thread, the more filament is consumed). Therefore, the path to be followed by the hotend to create a layer (L_C) is always the same, since the surface to be covered and the diameter of the nozzle are also the same. This value is provided by $L_{filament}$ and H-values, corresponding for each disc, and for all of them the same L_C value is obtained ($d_{filament}$ and d_{nozzle} are fixed values). So, for the case of this study:

$$t = \frac{L_C \cdot h_m}{S \cdot H} = \frac{986.4\ mm \cdot 1\ mm}{S \cdot H} = \frac{986.4\ mm^2}{S \cdot H} \quad (13)$$

The following procedure is an example of the utility of this relationship when, for instance, an A-value is imposed. Starting from the equation obtained to predict the behaviour of parameter A (eq. 5) and rearranging:

$$S = \frac{-A + 11224.0 + 3617.2 \cdot T - 2881.0 \cdot H - 1355.1 \cdot T^2}{2710.2} \quad (14)$$

Thus, for each pair of given H-T values and for a certain fixed value of A, S can be calculated. Subsequently, by substituting each calculated S-value and their corresponding H-values in the eq. 13, the printing time, t, is obtained.

It is important at this point to notice that, in eq. 13, the real values of variables S and H are entered, while, in eq. 14, it is necessary to use the normalized values of H and T between -1.682 and +1.682. Likewise, the printing speed values calculated from this equation also correspond to the normalised scale. Also, it is worth mentioning that fixed constant levels of H have been considered in this study, instead of S-values, because the layer height determines the resolution of the final 3D printed product and could, in some cases, be of interest for the optimisation of the printing process. However, when working with this kind of viscoelastic materials and in applications where the resolution of the final 3D object is not decisive, S instead of H may be chosen, following then the same procedure. Thus, for a given value of A (defined by product specifications), a new table can be elaborated from eqs. 13 and 14 (see selected values in Table S1, in the "Supporting Information" document), which in this case has been calculated for A = 12000 $Pa \cdot s^{1/z}$. Using these values, different curves can be plotted (Fig. 5), from which the time and temperature required to obtain a gel with an imposed A-value can be determined. If there would be any restriction to raise the temperature (degradation of some component, for example), by drawing a horizontal line from that value, the first crossing with any of the plotted curves will indicate the minimum printing time that will be used in the process to achieve a target rheological parameter, a value of A=12000 $Pa \cdot s^{1/z}$ in this example. On the contrary, if it is time that determines, for example, whether it is profitable to print a certain product in 3D, the procedure would be the inverse: it could be determined what would be the minimum temperature value that could be used and, therefore, the associated energy consumption.

5. Concluding remarks

3D printed κ-carrageenan gels were successfully obtained by means of a RepRap 3D printer, which was modified to be able to in situ gellify carrageenan-in-water dispersions. Thus printed gels can be obtained in a few minutes, exhibiting a rheological response comparable to that prepared conventionally by a process of 2 h duration. This seems to mean that, in spite of how briefly the material is inside the 3D printer, it is sufficient for the different transitions necessary for the development of the gel network.

Moreover, the multivariate analysis carried out on SAOS parameters obtained for 3D printed κ-carrageenan allowed to determine the effect of the main printing parameters (layer height, printing speed and hotend temperature) on the rheological response of gel structures created during printing process. In general, it can be concluded that an elevated temperature, together with a reduced velocity and layer height, favours the structuring of carrageenan, giving rise to gel networks with more intense interactions.

Based on this data and taking into account the influence of speed and layer height on printing time, an example of optimization of printing variables for obtaining a final product with a given specification has been presented.

6. References

Antunes, F. E., Coppola, L., Rossi, C. O., & Ranieri, G. A. (2008). Gelation of charged bio-nanocompartments induced by associative and non-associative polysaccharides. *Colloids and Surfaces B: Biointerfaces*, *66*(1), 134–140. https://doi.org/10.1016/j.colsurfb.2008.06.004

Ayuntamiento de Huelva. (2015). Agua potable y parámetros de calidad del agua semanal. Retrieved June 22, 2018, from http://www.aguashuelva.com/ESP/191.asp

Basu, S., Shivhare, U. S., Singh, T. V., & Beniwal, V. S. (2011). Rheological, textural and spectral characteristics of sorbitol substituted mango jam. *Journal of Food Engineering*, *105*(3), 503–512. https://doi.org/10.1016/j.jfoodeng.2011.03.014

Campo-Deaño, L., & Tovar, C. (2009, October 1). The effect of egg albumen on the viscoelasticity of crab sticks made from Alaska Pollock and Pacific Whiting surimi. *Food Hydrocolloids*. Elsevier. https://doi.org/10.1016/j.foodhyd.2009.03.013

Cavallieri, A. L. F., Fialho, N. A. V., & Cunha, R. L. (2011). Sodium caseinate and κ-carrageenan interactions in acid gels: Effect of polysaccharide dissolution temperature and sucrose addition. *International Journal of Food Properties*, *14*(2), 251–263. https://doi.org/10.1080/10942910903176345

469 Chinga-Carrasco, G., Ehman, N. V., Pettersson, J., Vallejos, M., Brodin, M., Felissia, F. E., … Area, M. C.
470 (2018). Pulping and pretreatment affect the characteristics of bagasse inks for 3D printing. *ACS*
471 *Sustainable Chemistry & Engineering*, *6*(3), 4068–4075.
472 https://doi.org/10.1021/acssuschemeng.7b04440
473 Cooke, M. E., Jones, S. W., ter Horst, B., Moiemen, N., Snow, M., Chouhan, G., … Grover, L. M.
474 (2018). Structuring of Hydrogels across Multiple Length Scales for Biomedical Applications.
475 *Advanced Materials*, *30*(14), 1705013. https://doi.org/10.1002/adma.201705013
476 ENAC. (2017). *Informe de análisis*. Retrieved from http://www.aguashuelva.com/DOC/01-02-
477 2018_Salida_Depsito_N1_2206179.pdf
478 Funami, T., Hiroe, M., Noda, S., Asai, I., Ikeda, S., & Nishinari, K. (2007). Influence of molecular
479 structure imaged with atomic force microscopy on the rheological behavior of carrageenan
480 aqueous systems in the presence or absence of cations. *Food Hydrocolloids*, *21*(4), 617–629.
481 https://doi.org/10.1016/j.foodhyd.2006.07.013
482 Gabriele, D., De Cindio, B., & D'Antona, P. (2001). A weak gel model for foods. *Rheologica Acta*,
483 *40*(2), 120–127. https://doi.org/10.1007/s003970000139
484 Gallegos, C., Brito-de la Fuente, E., Clavé, P., Costa, A., & Assegehegn, G. (2017). Nutritional Aspects
485 of Dysphagia Management. *Advances in Food and Nutrition Research*, *81*, 271–318.
486 https://doi.org/10.1016/BS.AFNR.2016.11.008
487 Godoi, F. C., Prakash, S., & Bhandari, B. R. (2016, June 1). 3d printing technologies applied for food
488 design: Status and prospects. *Journal of Food Engineering*. Elsevier.
489 https://doi.org/10.1016/j.jfoodeng.2016.01.025
490 Hermansson, A. M., Eriksson, E., & Jordansson, E. (1991). Effects of potassium, sodium and calcium
491 on the microstructure and rheological behaviour of kappa-carrageenan gels. *Carbohydrate*
492 *Polymers*, *16*(3), 297–320. https://doi.org/10.1016/0144-8617(91)90115-S
493 Holland, S., Tuck, C., & Foster, T. (2018). Fluid Gels: a New Feedstock for High Viscosity Jetting. *Food*
494 *Biophysics*, *13*(2), 175–185. https://doi.org/10.1007/s11483-018-9523-x
495 Iijima, M., Takahashi, M., Hatakeyama, T., & Hatakeyama, H. (2013). Detailed investigation of gel-sol
496 transition temperature of κ-carrageenan studied by DSC, TMA and FBM. *Journal of Thermal*
497 *Analysis and Calorimetry*, *114*(2), 895–901. https://doi.org/10.1007/s10973-013-2953-2
498 Ikeda, S., & Nishinari, K. (2001). "Weak gel"-type rheological properties of aqueous dispersions of
499 nonaggregated κ-carrageenan helices. *Journal of Agricultural and Food Chemistry*, *49*(9), 4436–
500 4441. https://doi.org/10.1021/jf0103065
501 Imeson, A. P. (2009). Carrageenan and furcellaran. In G. O. Phillips & P. A. Williams (Eds.), *Handbook*
502 *of Hydrocolloids: Second Edition* (pp. 164–185). Boca Raton: Elsevier.

https://doi.org/10.1533/9781845695873.164

Izdebska, J., & Zołek-Tryznowska, Z. (2016). 3D food printing - Facts and future. *Agro Food Industry Hi-Tech*, *27*(2), 33–37. Retrieved from http://www.teknoscienze.com/Contents/Riviste/PDF/AF2_2016_low_35-40.pdf

Jose, R. R., Rodriguez, M. J., Dixon, T. A., Omenetto, F., & Kaplan, D. L. (2016). Evolution of Bioinks and Additive Manufacturing Technologies for 3D Bioprinting. *ACS Biomaterials Science and Engineering*, *2*(10), 1662–1678. https://doi.org/10.1021/acsbiomaterials.6b00088

Kreiger, M., & Pearce, J. M. (2013). Environmental life cycle analysis of distributed three-dimensional printing and conventional manufacturing of polymer products. *ACS Sustainable Chemistry and Engineering*, *1*(12), 1511–1519. https://doi.org/10.1021/sc400093k

Lipton, J. I., Cutler, M., Nigl, F., Cohen, D., & Lipson, H. (2015). Additive manufacturing for the food industry. *Trends in Food Science and Technology*, *43*(1), 114–123. https://doi.org/10.1016/j.tifs.2015.02.004

Liu, S., Chan, W. L., & Li, L. (2015). Rheological Properties and Scaling Laws of κ-Carrageenan in Aqueous Solution. *Macromolecules*, *48*(20), 7649–7657. https://doi.org/10.1021/acs.macromol.5b01922

Liu, S., Huang, S., & Li, L. (2016). Thermoreversible gelation and viscoelasticity of κ-carrageenan hydrogels. *Journal of Rheology*, *60*(2), 203–214. https://doi.org/10.1122/1.4938525

Lupi, F. R., Gentile, L., Gabriele, D., Mazzulla, S., Baldino, N., & de Cindio, B. (2015). Olive oil and hyperthermal water bigels for cosmetic uses. *Journal of Colloid and Interface Science*, *459*, 70–78. https://doi.org/10.1016/j.jcis.2015.08.013

Mangione, M. R., Giacomazza, D., Bulone, D., Martorana, V., & San Biagio, P. L. (2003). Thermoreversible gelation of κ-Carrageenan: Relation between conformational transition and aggregation. *Biophysical Chemistry*, *104*(1), 95–105. https://doi.org/10.1016/S0301-4622(02)00341-1

Mita, T., & Bohlin, L. (1983). Shear stress relaxation of chemically modified gluten. *Cereal Chemistry*, *60*(2), 93–97. Retrieved from http://ci.nii.ac.jp/naid/80001616483/en/

Moresi, M., Bruno, M., & Parente, E. (2004). Viscoelastic properties of microbial alginate gels by oscillatory dynamic tests. *Journal of Food Engineering*, *64*(2), 179–186. https://doi.org/10.1016/j.jfoodeng.2003.09.030

Moxon, S. R., Cooke, M. E., Cox, S. C., Snow, M., Jeys, L., Jones, S. W., … Grover, L. M. (2017). Suspended Manufacture of Biological Structures. *Advanced Materials*, *29*(13), 1605594. https://doi.org/10.1002/adma.201605594

Munarin, F., Petrini, P., Barcellona, G., Roversi, T., Piazza, L., Visai, L., & Tanzi, M. C. (2014). Reactive

hydroxyapatite fillers for pectin biocomposites. *Materials Science and Engineering: C*, *45*, 154–161. https://doi.org/10.1016/J.MSEC.2014.09.003

Norton, I. T., Goodall, D. M., Morris, E. R., & Rees, D. A. (1983). Equilibrium and dynamic studies of the disorder-order transition of kappa carrageenan. *Journal of the Chemical Society, Faraday Transactions 1: Physical Chemistry in Condensed Phases*, *79*(10), 2489–2500. https://doi.org/10.1039/F19837902489

Pallottino, F., Hakola, L., Costa, C., Antonucci, F., Figorilli, S., Seisto, A., & Menesatti, P. (2016). Printing on Food or Food Printing: a Review. *Food and Bioprocess Technology*, *9*(5), 725–733. https://doi.org/10.1007/s11947-016-1692-3

Pearce, J. M., Morris Blair, C., Laciak, K. J., Andrews, R., Nosrat, A., & Zelenika-Zovko, I. (2010). 3-D Printing of Open Source Appropriate Technologies for Self-Directed Sustainable Development. *Journal of Sustainable Development*, *3*(4), 17–29. https://doi.org/10.5539/jsd.v3n4p17

Piculell, L. (2006). Gelling carrageenans. In A. M. Stephen, G. O. Phillips, & P. A. Williams (Eds.), *Food Polysaccharides and Their Applications* (2nd ed., pp. 239–287). Boca Raton: CRC Press.

Ren, X., Shao, H., Lin, T., & Zheng, H. (2016). 3D gel-printing-An additive manufacturing method for producing complex shape parts. *Materials and Design*, *101*, 80–87. https://doi.org/10.1016/j.matdes.2016.03.152

Rochas, C., & Rinaudo, M. (1982). Calorimetric determination of the conformational transition of kappa carrageenan. *Carbohydrate Research*, *105*(2), 227–236. https://doi.org/10.1016/S0008-6215(00)84970-8

Ross-Murphy, S. B., & Shatwell, K. P. (1993). Polysaccharide strong and weak gels. *Biorheology*, *30*(3–4), 217–227. Retrieved from http://www.ncbi.nlm.nih.gov/pubmed/8286724

Severini, C., & Derossi, A. (2016). Could the 3D Printing Technology be a Useful Strategy to Obtain Customized Nutrition? *Journal of Clinical Gastroenterology*, *50*(December), S175–S178. https://doi.org/10.1097/MCG.0000000000000705

Sun, J., Peng, Z., Zhou, W., Fuh, J. Y. H., Hong, G. S., & Chiu, A. (2015). A Review on 3D Printing for Customized Food Fabrication. *Procedia Manufacturing*, *1*, 308–319. https://doi.org/10.1016/j.promfg.2015.09.057

Sun, J., Zhou, W., Huang, D., Fuh, J. Y. H., & Hong, G. S. (2015). An Overview of 3D Printing Technologies for Food Fabrication. *Food and Bioprocess Technology*, *8*(8), 1605–1615. https://doi.org/10.1007/s11947-015-1528-6

Sun, J., Zhou, W., Yan, L., Huang, D., & Lin, L. ya. (2018). Extrusion-based food printing for digitalized food design and nutrition control. *Journal of Food Engineering*, *220*, 1–11. https://doi.org/10.1016/j.jfoodeng.2017.02.028

571 Tanaka, F. (2003). Thermoreversible Gelation Driven by Coil-to-Helix Transition of Polymers.
572 *Macromolecules*, *36*(14), 5392–5405. https://doi.org/10.1021/ma021688y
573 Tecante, A., & Doublier, J. L. (1999). Steady flow and viscoelastic behavior of crosslinked waxy corn
574 starch-κ-carrageenan pastes and gels. *Carbohydrate Polymers*, *40*(3), 221–231.
575 https://doi.org/10.1016/S0144-8617(99)00057-0
576 Thrimawithana, T. R., Young, S., Dunstan, D. E., & Alany, R. G. (2010). Texture and rheological
577 characterization of kappa and iota carrageenan in the presence of counter ions. *Carbohydrate*
578 *Polymers*, *82*(1), 69–77. https://doi.org/10.1016/j.carbpol.2010.04.024
579 Turcanu, M., Siegert, N., Secouard, S., Brito-de la Fuente, E., Balan, C., & Gallegos, C. (2018). An
580 alternative elongational method to study the effect of saliva on thickened fluids for dysphagia
581 nutritional support. *Journal of Food Engineering*, *228*, 79–83.
582 https://doi.org/10.1016/J.JFOODENG.2018.02.015
583 Vancauwenberghe, V., Katalagarianakis, L., Wang, Z., Meerts, M., Hertog, M., Verboven, P., …
584 Nicolaï, B. (2017). Pectin based food-ink formulations for 3-D printing of customizable porous
585 food simulants. *Innovative Food Science and Emerging Technologies*, *42*, 138–150.
586 https://doi.org/10.1016/j.ifset.2017.06.011
587 Wang, L., Zhang, M., Bhandari, B., & Yang, C. (2018). Investigation on fish surimi gel as promising
588 food material for 3D printing. *Journal of Food Engineering*, *220*, 101–108.
589 https://doi.org/10.1016/j.jfoodeng.2017.02.029
590 Wegrzyn, T. F., Golding, M., & Archer, R. H. (2012). Food Layered Manufacture: A new process for
591 constructing solid foods. *Trends in Food Science and Technology*, *27*(2), 66–72.
592 https://doi.org/10.1016/j.tifs.2012.04.006
593 Wittbrodt, B. T., Glover, A. G., Laureto, J., Anzalone, G. C., Oppliger, D., Irwin, J. L., & Pearce, J. M.
594 (2013). Life-cycle economic analysis of distributed manufacturing with open-source 3-D
595 printers. *Mechatronics*, *23*(6), 713–726. https://doi.org/10.1016/j.mechatronics.2013.06.002
596 Yang, Z., Yang, H., & Yang, H. (2017). Effects of sucrose addition on the rheology and microstructure
597 of κ-carrageenan gel. *Food Hydrocolloids*, *75*, 164–173.
598 https://doi.org/10.1016/j.foodhyd.2017.08.032
599 Zhu, F., Cheng, L., Yin, J., Wu, Z. L., Qian, J., Fu, J., & Zheng, Q. (2016). 3D Printing of Ultratough
600 Polyion Complex Hydrogels. *ACS Applied Materials and Interfaces*, *8*(45), 31304–31310.
601 https://doi.org/10.1021/acsami.6b09881
602

603 **Figure captions**

604 **Figure 1.** Schematic view of 3D printing setup to promote the in situ temperature-induced
605 gelification.

606 **Figure 2.** Star-shaped 3D printed κ-carrageenan gel model, (a) before and (c) after introducing the air
607 distributor cooling ring (b).

608 **Figure 3.** Evolution of storage (G') and loss (G") moduli with angular frequency of 3D printed and
609 conventionally prepared κ-carrageenan gel samples, as a function of (a) temperature, (b) layer
610 height and (c) printing speed.

611 **Figure 4.** Values of A and z parameters as a function of printing variables at different levels of (a,b)
612 layer height, (c,d) printing speed and (e,f) hotend temperature.

613 **Figure 5.** Time-temperature relationship for obtaining, by means of 3D printing, κ-carrageenan gels
614 with an imposed A value of 12000 $Pa \cdot s^{1/z}$.

615

616 **Table 1.** Independent variables studied and their normalised values used in the experimental design.

617

Printing speed [mm/s]	Hotend temperature [°C]	Layer height [mm]	Normalised value
10.0	50	0.06	-1.682
20.1	62	0.11	-1
35.0	80	0.18	0
49.9	98	0.25	1
60.0	110	0.30	1.682

618

619

620 **Table 2.** Fitting parameters A and z obtained for each case study as a function of printing variables.

621

Case	Normalised values of independent variables			A [Pa·s$^{1/z}$]	z	R^2
	S	T	H			
A	-1	-1	-1	13859.7	17.22	0.99
B	1	-1	-1	9719.1	17.89	0.99
C	-1	1	-1	18665.8	16.02	0.99
D	1	1	-1	12893.5	16.52	0.99
E	-1	-1	1	7444.0	13.91	0.97
F	1	-1	1	1662.3	12.11	0.95
G	-1	1	1	11754.5	15.36	0.98
H	1	1	1	7643.3	13.38	0.98
I	-1.682	0	0	15772.4	18.39	0.99
J	1.682	0	0	9593.0	15.44	0.99
K	0	-1.682	0	878.6	12.52	0.97
L	0	1.682	0	14506.7	13.28	0.99
M	0	0	-1.682	15125.7	18.19	0.99
N	0	0	1.682	7919.0	14.82	0.99
O1	0	0	0	10409.2	17.74	0.99
O2	0	0	0	9359.1	17.21	0.97
O3	0	0	0	10130.2	21.64	0.98
O4	0	0	0	11920.5	17.18	0.99
O5	0	0	0	11651.2	15.97	0.98
O6	0	0	0	11147.4	15.92	0.98

622

623

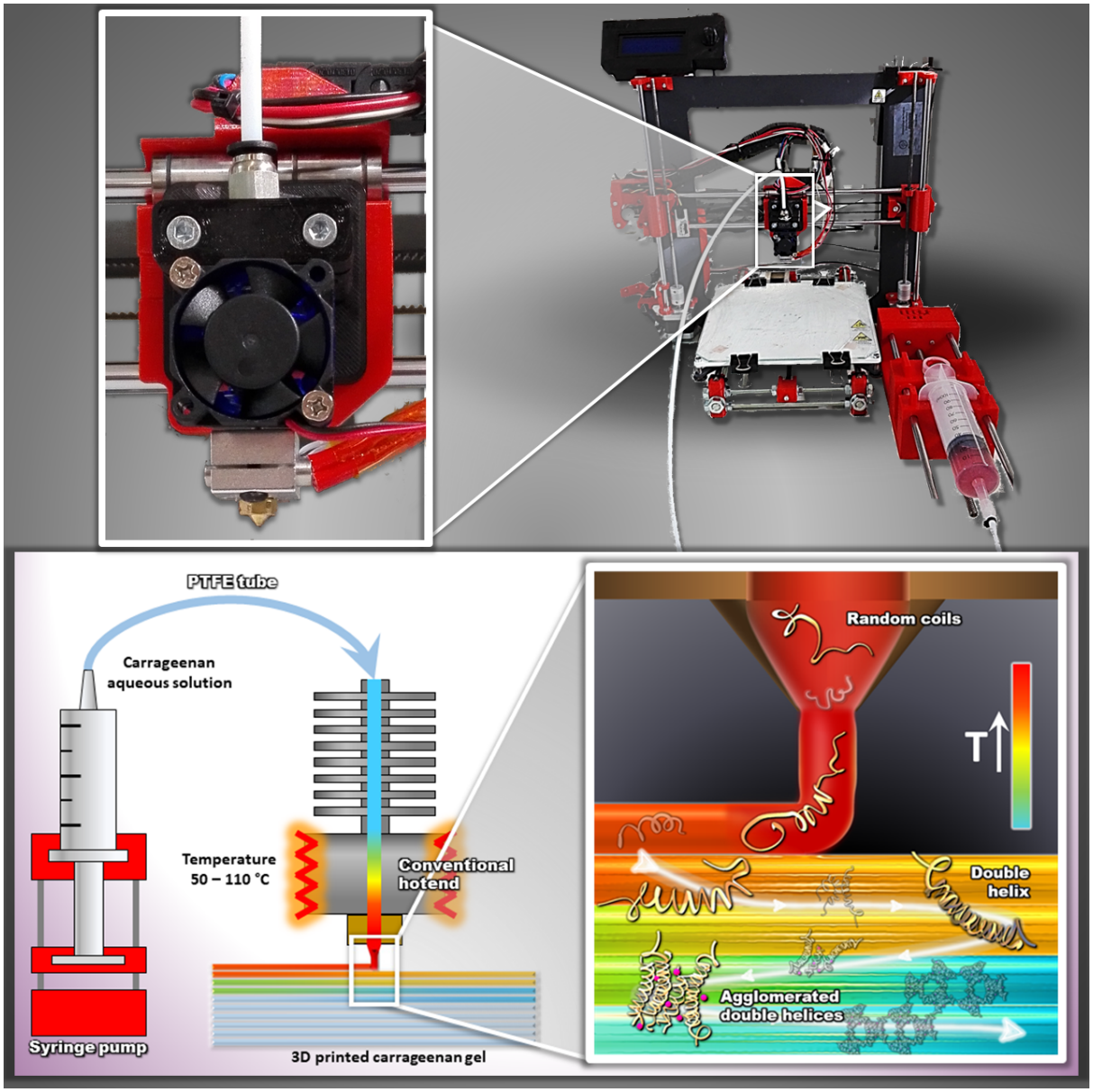

624

625 Figure 1.

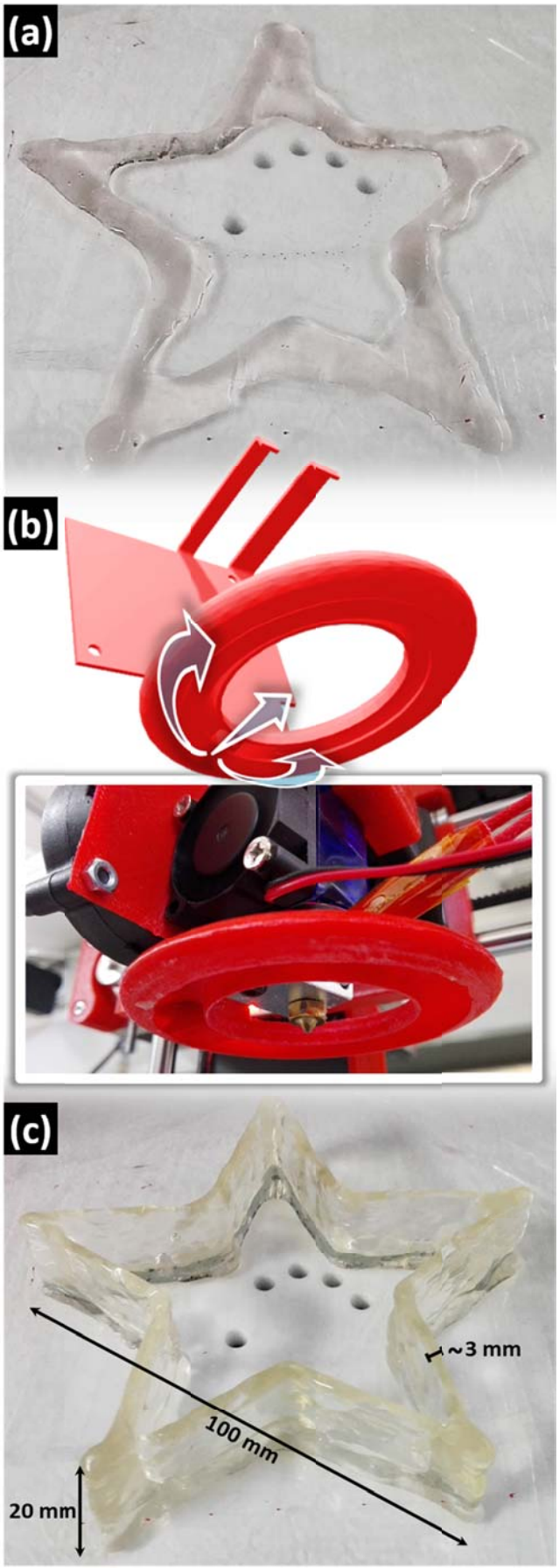

Figure 2.

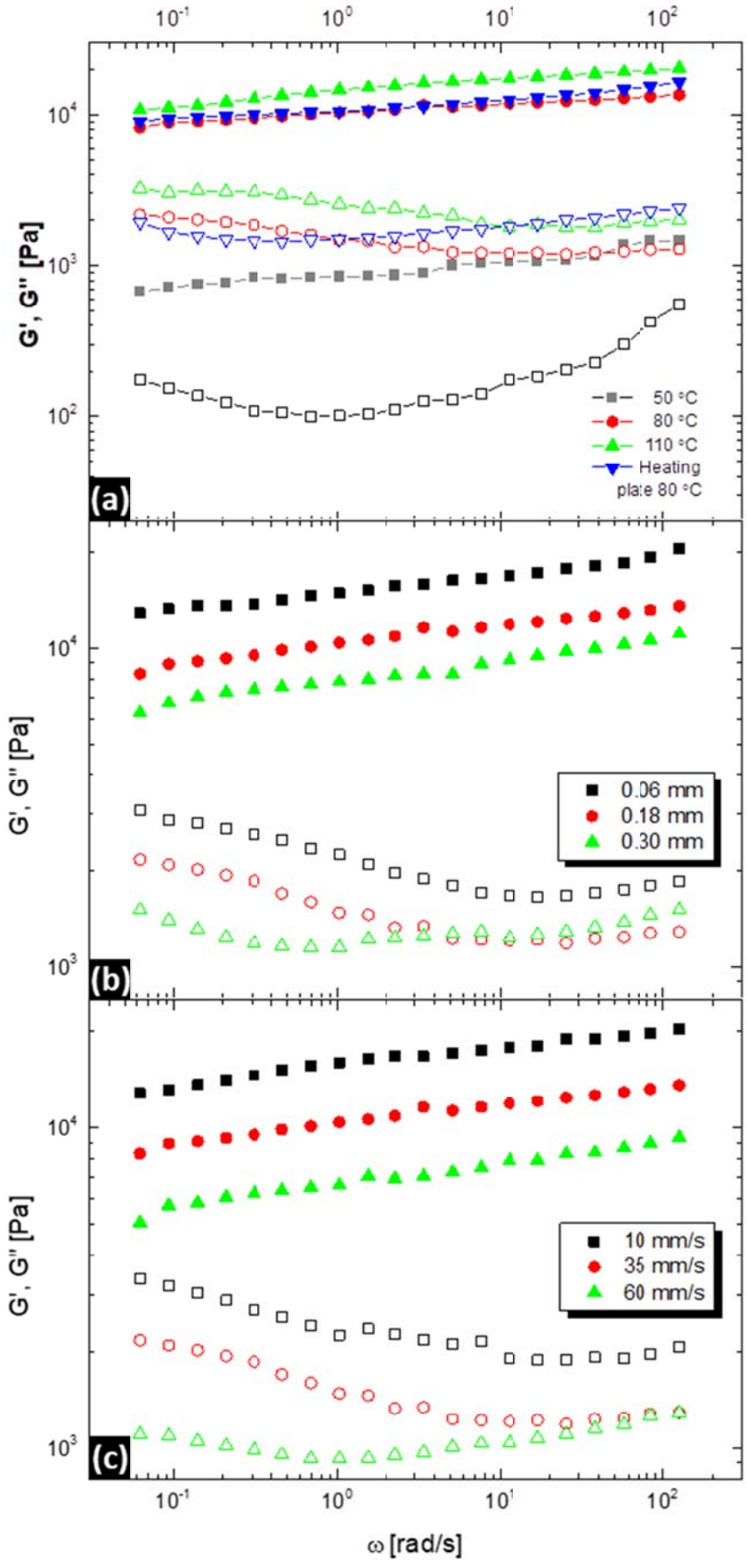

628

629 Figure 3.

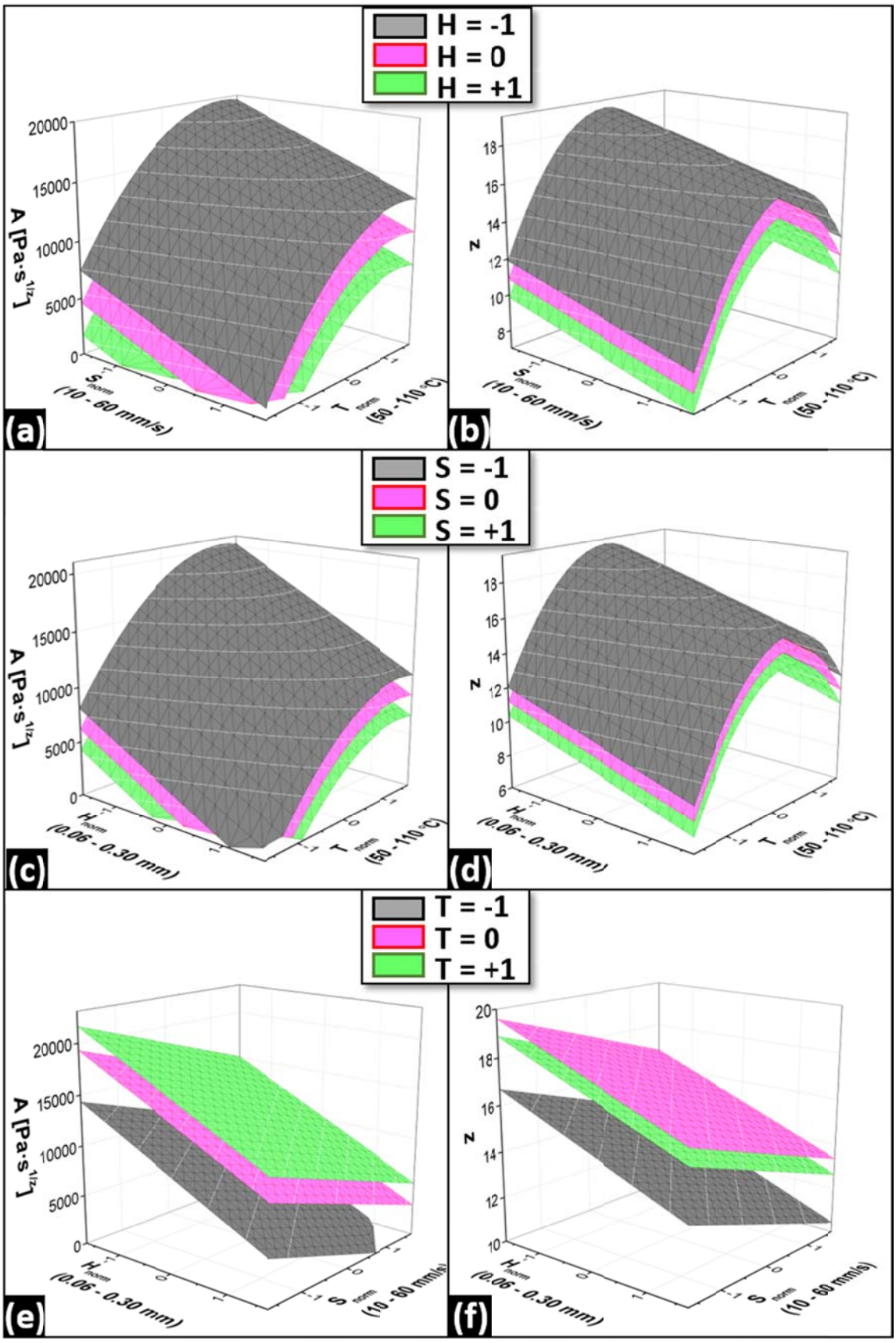

630

631 Figure 4.

632

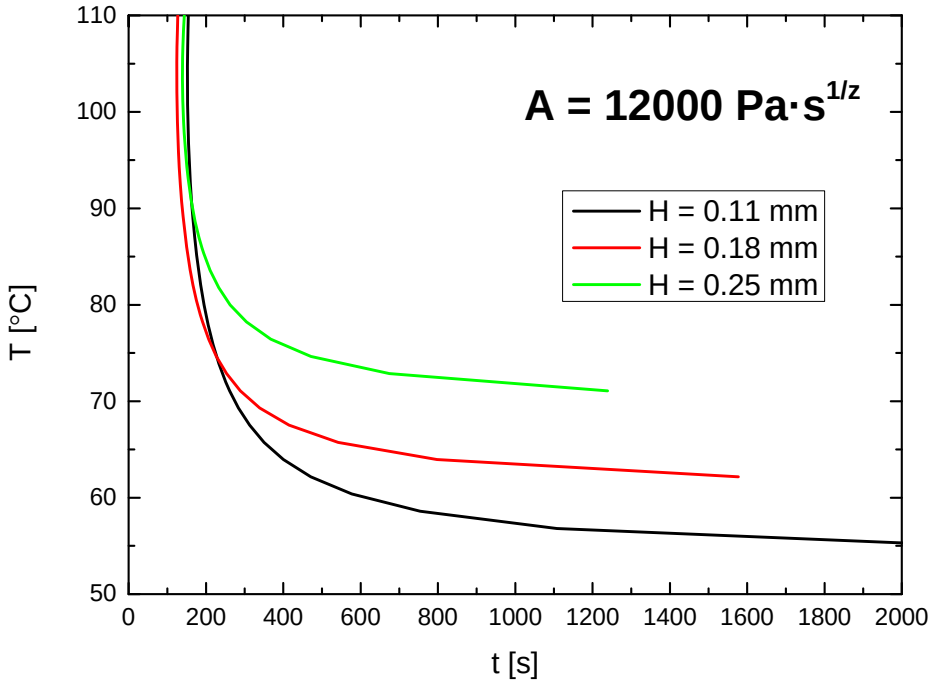

633

634 Figure 5.